Liquid-Absorbing System-Assisted Intersecting Jets Printing of Soft Structures from Reactive Biomaterials

Shinichi Sakurada[1,*], Marc Sole-Gras[2,*], Kyle Christensen[2], David B. Wallace[3], Yong Huang[1,2,4,**]

[1]Department of Biomedical Engineering, University of Florida, Gainesville, Florida 32611, USA

[2]Department of Mechanical and Aerospace Engineering, University of Florida, Gainesville, Florida 32611, USA

[3]MicroFab Technologies, Plano, TX 75074, USA

[4]Department of Materials Science and Engineering, University of Florida, Gainesville, FL 32611, USA.

*Equal contribution

[**]Corresponding author, Department of Mechanical and Aerospace Engineering, University of Florida, Gainesville, FL 32611, USA, Phone: 001-352-392-5520, Fax: 001- 352-392-7303, Email: yongh@ufl.edu

Abstract

Traditional three-dimensional (3D) bioprinting techniques of reactive materials usually include a mixing step of reactive agents prior to deposition, leading to potential changes in the rheological and biocompatibility properties of the resulting ink. During intersecting jets printing, reactive materials are dispensed separately, colliding and mixing with each other in air before landing on a previously deposited layer. While this enables reactive material printing using a printing-then-

mixing approach, the resulting excess fluid may compromise the printing quality and accuracy. This study aims to improve the performance of intersecting jets–based reactive material printing by introducing a stainless-steel wire mesh and fibrous tissue paper–based liquid-absorbing system, which functions as a method to remove the excess resultant liquid from the printing zone. The proposed stainless-steel wire mesh and tissue paper-based liquid absorbing system effectively absorbs the excess liquid resulted during the printing process which enables higher-resolution and denser depositions of soft structures. By selecting a proper wire mesh, the proposed liquid-absorbing system can absorb up to 65-90% of the excess liquid (water herein) resulting from printing aqueous reactive sodium alginate and calcium chloride inks, which are selected as model materials in this study. By controlling the tilt angles of intersecting jets, the incident angle of post-collision droplets is desirable to be less than 14º to avoid droplet bouncing on the top of a previously deposited layer during 3D bioprinting. Using the liquid-absorbing system, different 3D structures have been successfully printed using intersecting jets printing. For tubular alginate constructs printed in air from sodium alginate and calcium chloride inks, a 2.5 height-diameter ratio can be achieved. The proposed printing technology does not influence the post-printing cell viability while printing 3T3 cells, demonstrating its promising potential for bioprinting applications.

Keywords: three-dimensional bioprinting; material jetting; inkjet; intersecting jets; reactive materials

1. Introduction

The use of three-dimensional (3D) printing, a layer-by-layer additive or deposition manufacturing process, has been growing for the past several decades and has now extended to fabricating prototypes as well as final products [1,2,3,4]. 3D printing technology has been used to fabricate complex structures, which are difficult or time consuming when produced by traditional manufacturing processes such as molding, machining, and so on. More and more applications for the fabrication of small quantity, functionalized, customized, and/or hybrid products beyond their geometrical complexity are being developed. Recently, 3D bioprinting has been increasingly utilized in various applications for tissue engineering [5], which has been advanced by recent progress in cell sources and biomaterials. With 3D bioprinting as a bottom-up fabrication approach, it is now possible to build 3D biological patterns with specific functionalities [5,6,7]. During 3D bioprinting, different kinds of cells and/or biomaterials can be precisely deposited onto different positions, resulting in heterogeneous structures such as scaffolds, multi-layered constructs, and vascular-like features.

Various fabrication technologies have been utilized towards the goal of 3D bioprinting, mainly including micro-extrusion [8,9,10], laser-induced forward transfer [11,12], and inkjet printing [13,14,15,16,17,18]. Among all these printing methods, inkjet printing, a typical material jetting process, is advantageous in fabricating accurate 3D patterns with precision on the order of 10 micrometers since it can precisely dispense a repetitively controlled volume of ink voxel-by-voxel in a drop-on-demand fashion. However, the range of permissible viscosity of inks has been widely recognized as the main limitation on inkjet technology [19,20,21]. Generally, inks with a viscosity higher than 25 mPa·s (cP) may negatively impact the printing quality as optimum

jetting conditions will not be achieved due to unstable jetting or clogging. During bioprinting, some biomaterials may be reactive to each other, and after mixing, their resulting viscosity can be too high for inkjetting due to chemical reactions and/or gelation. For the printing of reactive materials, it is preferable to mix after printing, which can be accomplished by simultaneous printing or printing-then-mixing as described in [22].

Simultaneous printing can be implemented using the concept of droplet/jet collision in air via different droplet/jet formation mechanisms such as microdispensers [23], inkjet printheads [22], and in-air microfluidics [18]. In particular, Christensen et al. [22] developed an intersecting jets-based bioprinting approach to print 3D structures from reactive materials as colliding droplets. Similarly, Visser et al. [18], produced encapsulated droplets using an in-air microfluidics technology, which were further utilized to fabricate freeforms from different materials by colliding droplet/jet onto a continuous liquid jet in air. If gelling reactive materials are used, they react in the form of a gelation process that results in the formation of building blocks, either as collided droplets [22] or as encapsulated droplets [18], for 3D structure printing. Reactive materials used for bioprinting are usually aqueous and may produce gelation-induced excess liquid (such as water). This excess liquid not only deteriorates the printing performance but may also jeopardize the functional quality of printed structures. Therefore, there is a need to remove this resulting excess liquid during the deposition process.

The objective of this research is to improve the performance of intersecting jets–based reactive material printing by introducing a stainless-steel wire mesh (SSWM) and fibrous tissue paper–based liquid-absorbing system, which functions as a method to remove the excess resultant liquid

from the printing zone. The effects this liquid removal system has on the printing process and its printing results are investigated. In particular, the effects on the printing process are investigated regarding the incident angle, droplet bouncing and part fidelity, whereas the bioprinting performance is characterized in terms of the printed cell viability and cell proliferation. The proposed intersecting jets-based printing capabilities can be utilized for direct biofabrication in air such as wound dressing printing for patients in need. For example, Skardal et al. [24] showed how direct printing of stem cells (i.e. amniotic delivered stem cells and bone marrow-derived mesenchymal stem cells) onto skin defects can lead to faster recovery times, and Lee et al. [25] showed the importance played by the cell position (keratinocytes and fibroblasts) on regenerating dermal and epidermal structures. It is envisioned that cellular patterns and constructs can be directly fabricated in air from reactive materials using intersecting jets printing, satisfying the bioprinting need for certain tissue engineering and regenerative medicine applications. While sodium alginate (NaAlg) and calcium chloride ($CaCl_2$) solutions are utilized as reactive materials in this study, the resulting knowledge applies to inks based on (aqueous) reactive materials.

2. Materials and Methods

2.1. Materials

Alginate, extracted from seaweed, is a common material for bioinks due to its wide applicability as a versatile biomaterial [16,26.27]. While alginate is an unideal material for living tissue construction, it is a good hydrogel material for proof-of-concept bioprinting studies. For the basic 3D printing experiment in this study, two alginate inks were utilized: aqueous 0.5% and 0.8% (w/v) sodium alginate (Acros, NJ, USA) inks, which were cross-linked by using two aqueous 5.0% and 20.0% (w/v) calcium chloride dehydrate (Sigma-Aldrich, St. Louis, MO,

USA) inks. Sodium alginate and calcium chloride solutions are reactive and form an alginate gel once mixed. Alginate primarily consists of a family of unbranched binary copolymers of α-L-guluronic acid (G blocks) and 1,4 linked β-D-mannuronic acid (M blocks). Two G blocks of adjacent alginate polymer chains can be cross-linked with multivalent cations such as calcium cations herein through interactions with carboxylic groups. It is noted that calcium chloride was successfully printed into a sodium alginate bath to print 3D constructs [28] and sodium alginate was successfully printed into a calcium chloride bath to print 3D constructs [16]. For this study, both sodium alginate and calcium chloride are dispersed from two different nozzles, collide and mix in air, and further build up 3D features.

For cell printing studies, NIH 3T3 mouse fibroblasts (ATCC, Rockville, MD) were used to prepare the bioink. The bioink was prepared by mixing a Dulbecco's modified Eagle's medium (DMEM)-based 0.5% (w/v) sodium alginate solution with 3T3 cells, which were obtained as previously reported [16]. The resulting cell density was 5×10^6 cells/mL. Using this bioink, 5.0 mm diameter tubular structures were printed.

2.2. Printing process

2.2.1. Setup of intersecting jets-based printing system

Herein 3D inkjet printing using intersecting jets is implemented by simultaneously ejecting two (or more) droplets using inkjetting that collide, mix, and react *in situ* over a receiving substrate to build 3D structures as previously reported [22]. Figure 1(a) shows an overview of the intersecting jets-based inkjet printing system. The setup can be divided into three main functions: droplet generation, droplet orientation control, and receiving substrate adjustment. Droplets were

generated using two 120 μm diameter ABL piezoelectric inkjet printheads (MicroFab, Plano, TX) with frequencies of 20–60 Hz, rise and fall times of 6 μs, dwell/echo times of 35–65 μs, and driving voltage between +/- 80V and +/- 85V, respectively. To maintain a desired meniscus level of inks, back pressure was applied by using a multichannel pneumatic controller (MicroFab, Plano, TX). Both jet trajectories were aligned to intersect by orienting the printheads to the corresponding tilt angles α and β (typically 0 - 30º), corresponding to Printheads 1 and 2, respectively, by using a customized goniometer (Thorlabs, Newton, NJ)-based apparatus. Specifically, Printhead 1 was used for alginate while Printhead 2 was used for calcium chloride printing.

The receiving substrate consisted of a liquid-absorbing system composed by a stainless-steel wire mesh/filter (McMaster-Carr, Douglasville, GA) and Kimwipes® tissue paper (Kimberly-Clark Professional, Roswell, GA) underneath as shown in Figure 1. The liquid-absorbing system was designed to absorb the excess liquid, such as water, that passed through the wire mesh due to gravity and was drained away via tissue paper. The wire mesh had a mesh size of 80, 100 and 200, corresponding to a nominal sieve opening of 177, 149, and 74 μm (0.0070”, 0.0055” and 0.0029”), respectively. Printhead motions were regulated by *xy* translational motion stages (Aerotech, Pittsburgh, PA) and the height of the receiving substrate was controlled by a *z* translational motion stage (Aerotech, Pittsburgh, PA) based on a computer aided design (CAD) model of printed structures as shown in Figure 1 (b). Printhead traveling speed operated from 1 to 10 mm/s.

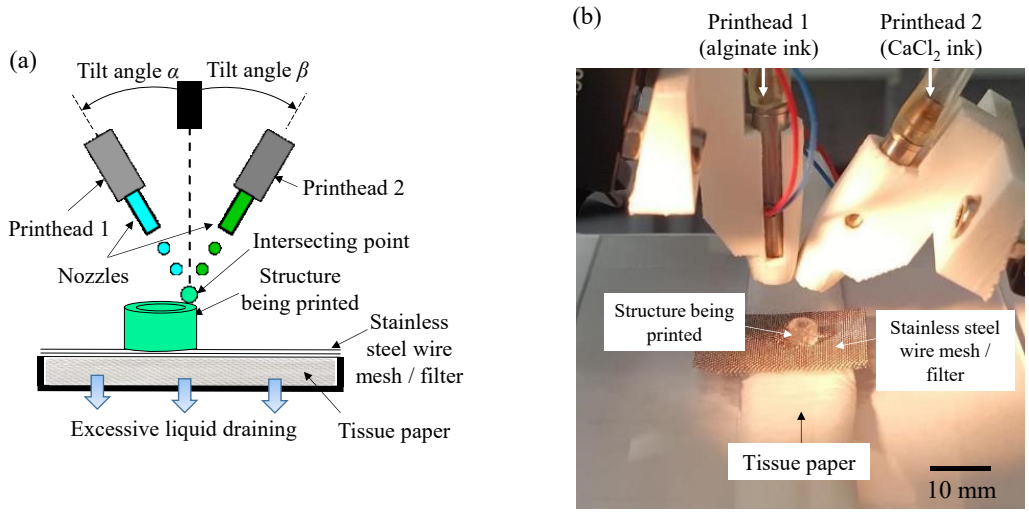

Figure 1. (a) Intersecting jets printing process and (b) printing setup

2.2.2. Design of printing experiments

Table 1 details the structures, materials, printing conditions, and dimensions adopted in this study. The maximum printable sodium alginate content was determined as 0.8% (w/v) as higher concentration alginate solutions clog the nozzle due to their higher viscosities. As such, 0.5% and 0.8% (w/v) sodium alginate solutions were used. Large 3D structure printing requires each structure to hold its own shape and weight, so adequate mechanical strength is required. For given materials, this can be achieved via fast gelation, which is obtained using calcium chloride content as high as 20.0 % (w/v) and/or tuning the printhead printing frequency of both printheads. Nevertheless, a high gelation speed might result in dried structures when exposed at room temperature for long times, leading to low cell viability. As such, calcium chloride was used in a lower concentration (5.0 % (w/v)) and ejected at a lower frequency (20 Hz) to retain more water in printed structures. It should be pointed out that the printing frequencies also determine the ratio between the quantities of deposited reactive materials and influence the

reaction speed, therefore the printing quality of resulting constructs. Either high or low reaction speed should be avoided, and the ratio of the sodium alginate droplets over the calcium chloride droplets herein was determined as 3:1 (that is, 60 Hz vs. 20 Hz) for the best printing performance. Different stainless-steel wire meshes were tested to identify the optimal wire opening based on the amount of drained liquid while printing 3 mm diameter circular tubular structures of variable heights.

Table 1. Design of intersecting jets printing experiments (with Printhead 1 printing frequency at 60 Hz)

<table>
<tr><th colspan="2" rowspan="2">Structure type</th><th colspan="2">Reactive materials (w/v%)</th><th rowspan="2">Liquid-absorbing system</th><th rowspan="2">Printhead 2 printing frequency</th><th colspan="2">Structure dimensions</th></tr>
<tr><th>Printhead 1 (Sodium alginate)</th><th>Printhead 2 (Calcium chloride)</th><th>Diameter (mm)</th><th>Height (mm)</th></tr>
<tr><td rowspan="6">Acellular structures (for validation and comparison)</td><td>Liquid-absorbing performance</td><td>0.8</td><td>20.0</td><td>With (using different mesh sizes)</td><td>60 Hz</td><td>3.0 mm</td><td>variable</td></tr>
<tr><td>Annular/ hexagonal</td><td>0.8</td><td>20.0</td><td>With</td><td></td><td></td><td>0.6 mm</td></tr>
<tr><td rowspan="4">Tube</td><td rowspan="2">0.5</td><td rowspan="2">5.0</td><td>Without</td><td>20 Hz</td><td rowspan="2">5.0 mm</td><td>1.5 mm</td></tr>
<tr><td>With</td><td>60 Hz</td><td>0.5 mm</td></tr>
<tr><td rowspan="2">0.8</td><td rowspan="2">20.0</td><td>Without</td><td>60 Hz</td><td rowspan="2">3.0 mm</td><td rowspan="2">10.0 mm</td></tr>
<tr><td>With</td><td>60 Hz</td></tr>
<tr><td>Cone</td><td>0.5</td><td>5.0</td><td>With</td><td>60 Hz</td><td>5.0 mm</td><td>5.4 mm</td></tr>
<tr><td rowspan="2">Cellular constructs</td><td rowspan="2">Tube</td><td rowspan="2">0.5 (alginate-based fibroblast suspension)</td><td rowspan="2">5.0</td><td>Without</td><td>20 Hz</td><td>5.0 mm</td><td>1.5 mm</td></tr>
<tr><td>With</td><td>60 Hz</td><td>5.0 mm</td><td>1.5 mm</td></tr>
</table>

To ensure the droplet collision, each drop formation process (mainly, in terms of the droplet speed) was adjusted by changing the dwell/echo times and excitation voltages. As illustrated in Figure 2(a), both reactive material droplets are ejected with different speeds (v_a and v_b in Figure 2(a1)) whose difference in magnitude determines not only the collided droplet speed (v_c in Figure 2(a2)) but also the moving direction of the resulted droplet in terms of the incident angle γ. Ejection velocities were determined to be 2.5-5 m/s in this study, and the resulting droplet directly landed on the previously deposited layer directly. Using a time-resolved imaging system (MicroFab, Plano, TX), the collision of two droplets (Figure 2(b)-(e)) can be observed and verified. The z displacement of the receiving substrate can also be adjusted accordingly in order to ensure that the collision location is atop of the previously printed layer as seen in Figure 2(d) and (e). The time gap between two consecutive depositions at 60 Hz is 16.7 ms, which is much shorter than the typical alginate layer gelation time (on the order of 1 second [12,29]) for a typical layer thickness (on the order of 10 μm) during bioprinting. This short time gap promotes effective collision, landing, and mixing of two colliding droplets before any gelation or encapsulation takes place. As reported, two materials can mix well during and after collision/landing [30]. After collision, landing, and mixing, deposited materials have enough time to cross-link and build up a homogeneously gelled structure instead of a stack of encapsulated droplets.

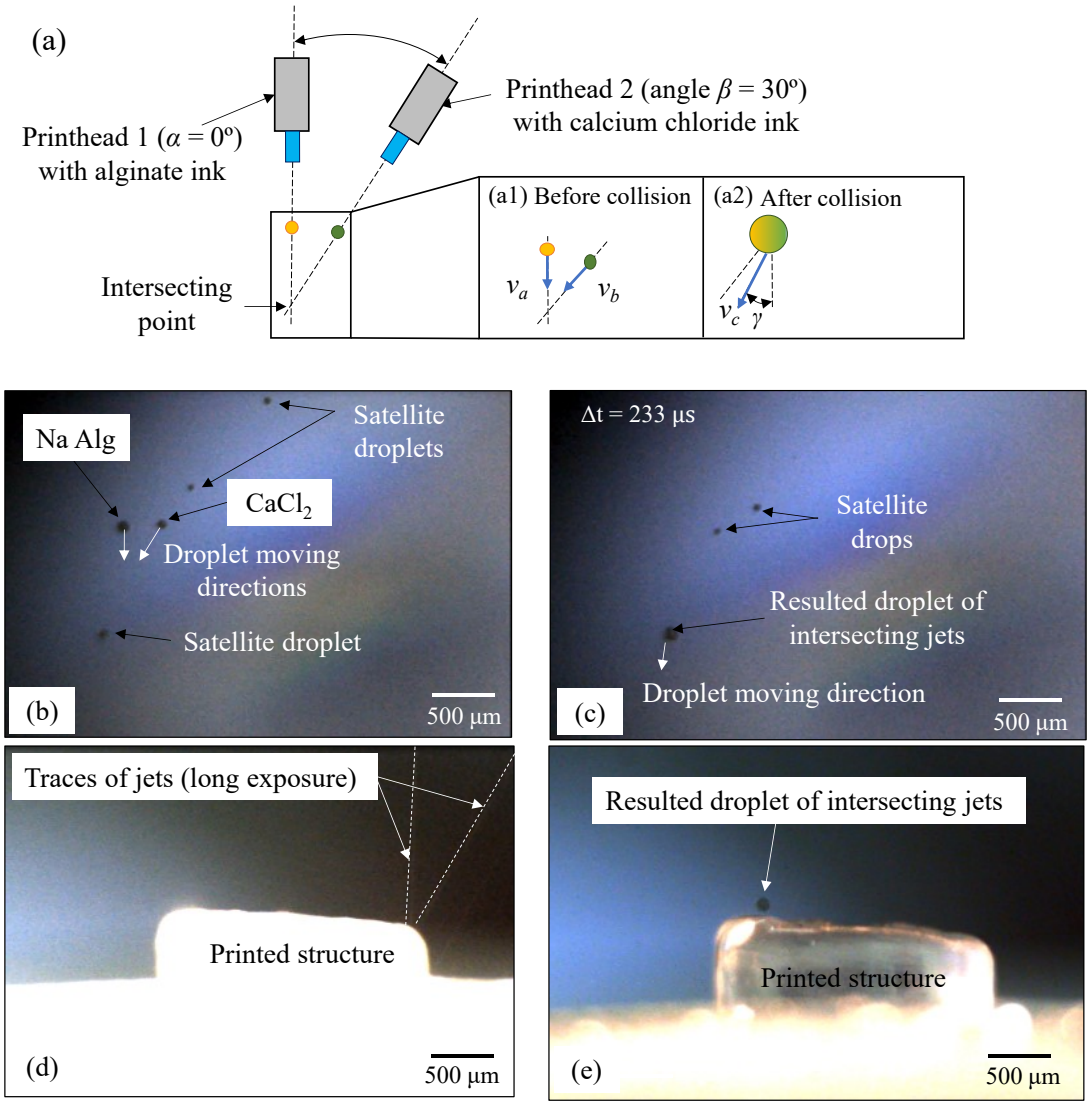

Figure 2. (a) Printing schematic and printing sequence illustrating the intersecting jets printing approach (insets: (a1) before and (a2) after collision), and images of droplets (b) before and (c) after collision, and (d) and (e) voxel-by-voxel printing process

2.3. Quantification of the incident angle effect

During the droplet landing process, there may be droplet bouncing instead of coalescing [31,32] due to a high landing velocity, which may affect the collision of intersecting jets-produced

droplets. Since there might be some time difference between intersecting jets-produced landing droplets, droplet bouncing should be minimized in order to have complete collision and mixing among droplets. As shown in Figure 3, the bouncing of droplets depends on the velocity and trajectory (or incident angle γ) of landing droplets, and the latter is determined based on the position of the printhead, which is configured to generate post-collision droplets to simulate the intersecting jets printing process. In order to experimentally identify the threshold of bouncing phenomena, printing was simulated as follows: deposition of a low concentration sodium alginate ink (0.5% (w/v)) onto a low concentration calcium chloride solution (5.0% (w/v)) to represent an alginate-based post-collision droplet landing onto a calcium chloride dominated receiving substrate. The Weber number was calculated as follows: $W_e = \frac{\rho v^2 l}{\sigma}$, where *We* is the Weber number, ρ is the density (kg/m^3), which is 1005 kg/m^3, v is the landing velocity (m/s) as measured based on the averaged distance over travel time, l is the characteristic length (m), which is the nozzle diameter (120 $\times 10^{-6}$ m), and σ is the surface tension (mN/m), which is 71.2 mN/m as measured by the pendant drop method using a tensiometer (Attension ThetaLite 101, Biolin Scientific, Sweden). The velocity vector was decomposed to v_x and v_y to consider each influence on the Weber number.

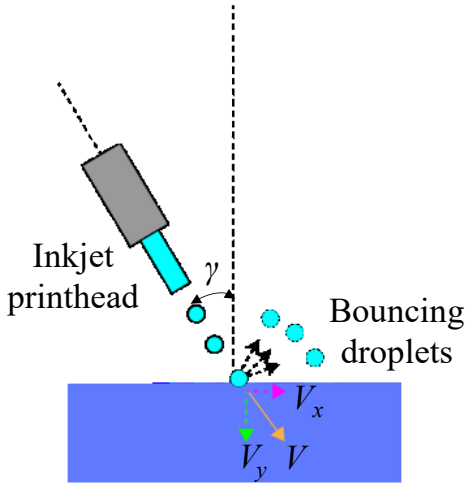

Figure 3. Schematic of the effect of incident angle on bouncing droplets

2.4. Cell viability and morphology

All constructs were transferred into a 24 well plate filled with 2 mL Dulbecco's modified Eagles medium (DMEM) (Corning Cellgro, Manassas, VA) after printing, which was supplemented with 10% FBS (GE Healthcare Life Science, Logan, UT). These printed samples were cultured for ten days at 37°C and 5 % CO_2, and the culture medium was changed on the fourth and seventh days after the cellular constructs were printed. Cell-laden constructs were washed with PBS (Fisher Scientific, Hanover Park, IL) once and then liquefied using sterile 1.62% sodium citrate (Sigma-Aldrich, St. Louis, MO). After centrifuge, the supernatant were pipetted out, and the pellets were stained with a final concentration of 10 µg/mL Hoechst 33342 (Sigma-Aldrich, St. Louis, MO) to stain nuclei blue, a final concentration of 10 µg/mL fluorescein diacetate (FDA) (Sigma-Aldrich, St. Louis, MO) to stain live cells green, and a final concentration of 2 µg/mL propidium iodide (PI) (Sigma-Aldrich, St. Louis, MO) to stain dead cells red in 50 µL PBS. The images were captured using an EVOS FL inverted fluorescence microscope (EVOS FL, ThermoFisher Scientific, Waltham, MA). For the observation of cell morphology, after

washing twice by PBS, the printed samples were stained by PBS with an FDA concentration of 10 μg/mL. Then, the cell morphology was observed using fluorescence microscopy after squashing the printed constructs between two microscope cover glasses.

2.5. Characterization of the absorbing performance of the liquid-absorbing system

Liquid absorption performance by the liquid-absorbing system was measured based on the weight difference of tissue paper before and after printing since the tissue paper absorbs all resulting excess water during printing and after gelation. In this study, the tissue paper was not changed during each printing process since the absorbed water was effectively drained away and distributed through the fibrous paper body due to the capillary effect.

3. Results and discussion

3.1. Effects of the Liquid-absorbing System on the Printing Process

3.1.1. Liquid-absorbing performance of stainless-steel wire mesh

In order to determine the liquid absorption performance of the proposed system, stainless-steel wire meshes with different opening sizes were tested along with tissue paper for different durations during tube printing as seen from Figure 4. The opening between wire mesh wires allows the excess water to pass through and be directly absorbed by the fibrous tissue paper beneath.

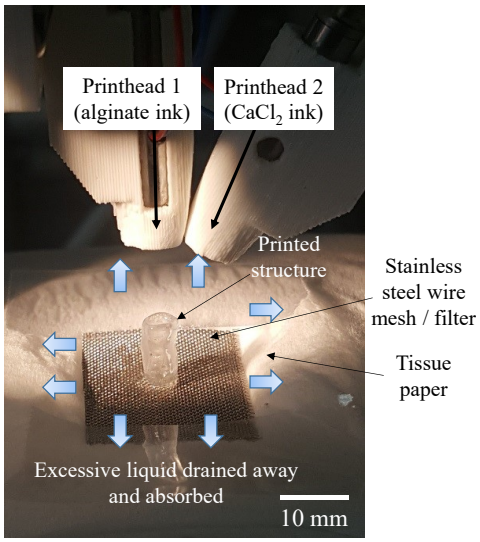

Figure 4. Example of tubular structure printing

Figure 5 shows the performance of the proposed liquid absorbing system in terms of the amount of absorbed liquid (Figure 5(a)), absorbing speed of the liquid (Figure 5(b)), and absorbing ratio of liquid (Figure 5(c)). It can be seen that the bigger the mesh opening area, the greater the amount of absorbed liquid, absorbing speed, and absorbing ratio by the system. For the mesh size 80 system, the amount of absorbed liquid (water herein) is approximately 0.20, 0.40 and 0.45 g after printing for 500, 1000, and 1500 seconds, correspondingly. A smaller mesh opening size system, such as the mesh size 100 system, results in a 15-20% lower amount of absorbed liquid at 500 and 1000 s. The absorption speed of the mesh size 80 and 100 systems decreases with printing time. The mesh size 80 system shows an absorbing speed of approximately 0.41, 0.38 and 0.31 mg/s (25, 23, and 19 mg/min) at 500, 1000 and 1500 s, respectively, whereas the 100 mesh size system absorbs 0.36, 0.31 and 0.30 mg/s (22, 19, and 18 mg/min) for printing times of 500, 1000 and 1500 s respectively. However, there is no significant difference of the absorption performance at 1500 s between these two systems. This may be attributed to the fact that a

decreased amount of the resulting water during printing reaches the absorbing zone, which is located at the bottom of structure/construct being printed, due to some evaporation when the resulting water flows down along a tall structure. As a result, the available water for absorption is limited and falls within the absorbing capacity of both systems at 1500 s. It is noted that even though a smaller wire mesh filter (mesh size 200, 74 μm) is able to absorb liquid at approximately 9 mg/min at the beginning of printing, its opening size is not large enough to effectively avoid the accumulation of excess liquid because the mesh opening does not allow most of the excess liquid to go through quickly after 500 s of printing, and no further testing for longer printing times has been carried out. Conversely, wire meshes with a bigger opening size larger than 177 μm (mesh size of 80) are not evaluated since an entire droplet may easily pass through the wire mesh instead of building up any structure on the top of the wire mesh.

Since both alginate and calcium chloride inks are aqueous and the excess liquid is also water, the absorption ratio is approximated based on the amount of absorbed liquid over the amount of deposited material, which can be estimated using the droplet diameter as obtained using the time-resolved imaging system. The mesh size 80 system can absorb approximately 89%, 82%, and 67% of the deposited material in form resulting in the form of excess liquid at 500, 1000, and 1500 s respectively, while the mesh 100 system can absorb 79%, 68% and 66%, respectively.

As observed, wire meshes with a wire opening between 149 and 177 μm (mesh size 100 and 80) are sufficient to allow 65-90% of the resulting excess liquid to drain through and be absorbed by the tissue paper under the printing zone. Given its higher absorption ratio for all printing times, the mesh size 80 system is identified as the best wire mesh for freeform printing since the

stainless-steel wire mesh and tissue paper underneath are capable of absorbing excess liquid during a typical 3D bioprinting duration (30 mins herein), enabling 3D printing of reactive materials.

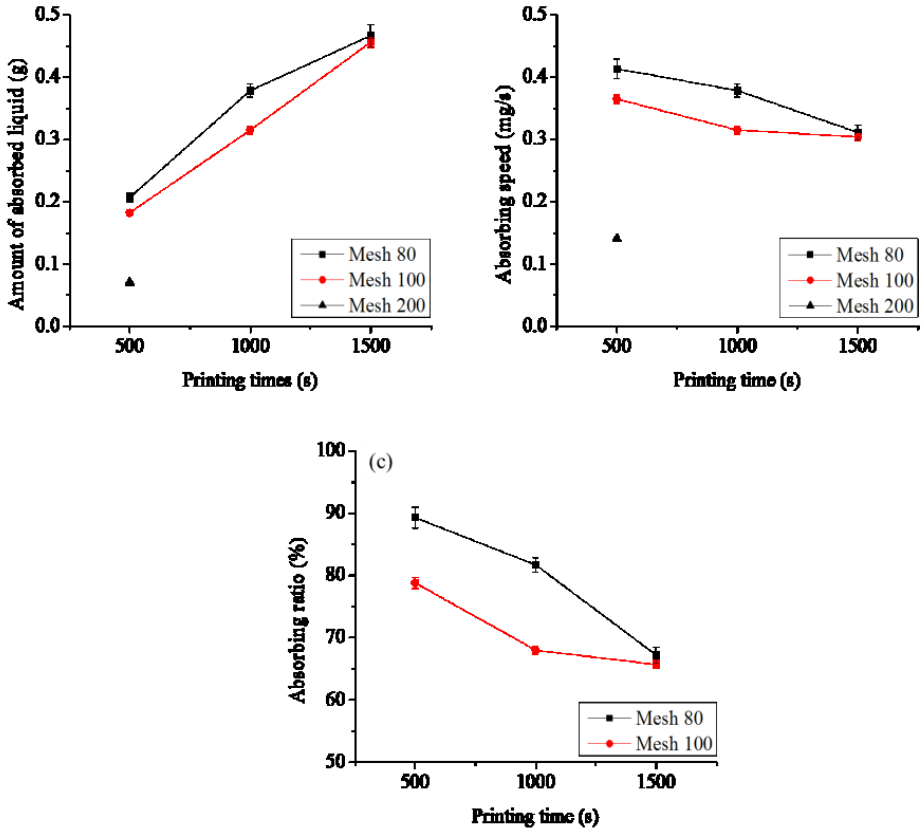

Figure 5. Absorbing performance of the liquid absorbing system in terms of (a) amount of absorbed liquid, (b) absorbing speed, and (c) absorbing ratio (error bar: +/- standard deviation)

3.1.2. Effect on incident angle on bouncing of droplets at the landing spot

To study droplets bouncing on the top of the surface of printed structures, a dark colored substrate was immersed 5 mm below the surface of a 5% (w/v) calcium chloride solution (Figure 6(a)) to easily observe the bouncing of incident alginate droplets to simulate the post-collision droplets. Examples of bouncing trajectories are outlined in black for visualization as seen from

Figure 6(a). As previously discussed, the Weber number along the x and y directions can be calculated based on the decomposed velocity vectors along the x-axis and y-axis, respectively as seen in Figure 3(b). As illustrated in Figure 6(b), increasing incident angle results in a higher Weber number and a lower Weber number in the x-axis and y-axis, respectively. Similar We number values were reported (≈12 - 22) [33] in the normal direction with respect to the surface when water droplets bounced on the top of a water flat surface. Since bouncing phenomena was observed at incident angles above 14°, the calculated We threshold numbers are 1.3 and 20.7 in the x and y directions. While coalescence conditions are desirable herein, it should be noted that bouncing phenomena may still appear under some coalescence conditions [34].

Since wetting conditions at the nozzle outlet may compromise the creation of stable jetting conditions due to printhead inclination, tilt angles α and β were set to 0 and 30º respectively, which resulted in an incident angle γ of approximately 5º for post-collision droplet deposition. This tilt angle configuration effectively prevents droplets from bouncing on the surface of the printed structure, leading to a more accurate deposition and therefore, a better printing resolution.

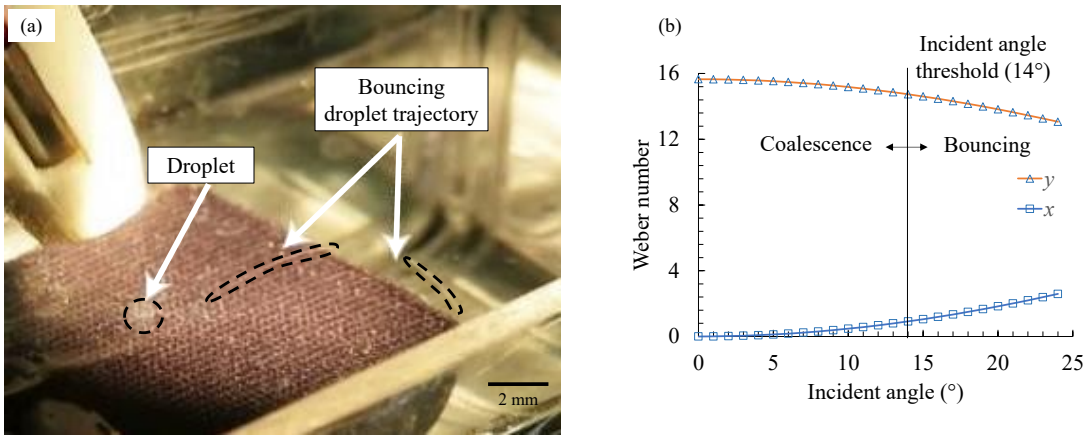

Figure 6. (a) Bouncing droplets on the surface of a 5.0% calcium chloride solution and (b) the relationship between the incident angle and Weber number

3.2. Effect on printing results

Figure 7(a) presents a printing result when using intersecting jets without the liquid-absorbing system in place [22]. By comparing the printing performance as seen from Figure 7(a) and (b), the liquid-absorbing system can effectively remove the excess liquid around the landing and deposition spot. Excess liquid, if present, around the printing zone may compromise not only the landing spot but also the structure integrity and material homogeneity of structures as seen from Figure 7(c). The excess liquid around a 3D structure interrupts direct landing of the intersected droplet onto a previous layer, preventing their merge. Under some circumstances it can also result in the formation of isolated alginate gel beads. Figure 7(d) depicts the liquid removal effect of the liquid-absorbing system when compared to regular intersecting jets printing on a non-porous substrate. An additional effect of using the liquid-absorbing liquid system is that the resulting structures are denser since some water is wicked away by the liquid-absorbing system, and the layer thickness of the 0.5% alginate ink decreases from 50 μm to 15 μm in this study.

Some representative printed results are shown in the following sections to demonstrate the effectiveness of the proposed liquid-absorbing system for intersecting jets printing.

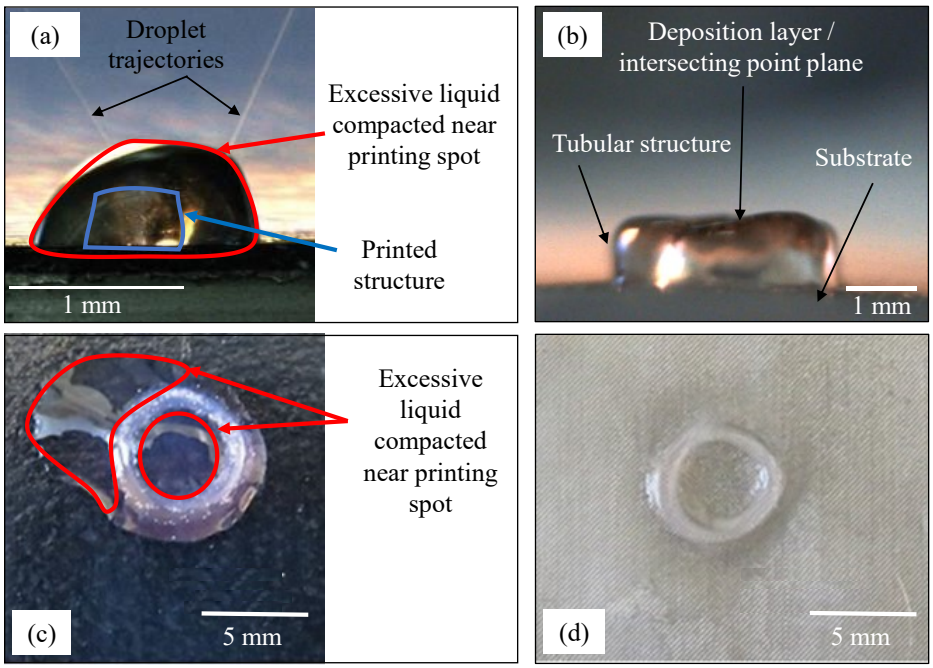

Figure 7. Time-resolved images of printing (a) without [22] (Reprinted (adapted) with permission from ACS Biomater. Sci. Eng. Copyright 2017 American Chemical Society) and (b) with the liquid-absorbing system. Comparison of a printed tubular construct with 3T3 cells without (c) and with (d) the liquid-absorbing system

By using the identified printing conditions (mesh size 80, printing speed of 1mm/s, and tilt angles α and β of 0º and 30º, respectively), different structures were printed by draining away the excess liquid resulting from the reaction of sodium alginate and calcium chloride solutions. Specifically, in order to demonstrate the improvement of printing performance, higher height-diameter ratio tubular structures with a diameter of 5.0 mm were fabricated with the liquid-absorbing system. The maximum tube height obtained when using the liquid-absorbing system is

approximately 10.0 mm. Tubular cellular constructs with 5.0 mm diameter and 1.5 mm height were printed with and without the liquid-absorbing system. Layer thickness is determined as 15 μm and 50 μm when the liquid-absorbing system is and is not used, respectively.

3.2.1. Annular/hexagonal structure

Alginate structures have been successfully printed using intersecting jets without any liquid-absorbing system [22], but the presence of water in the printing zone has affected the sharpness of the edges, resulting in uniform cross sections along the circumferential direction as seen from Figure 8(a). By using the liquid-absorbing system, annular/hexagonal honeycomb structures with sharper and well-defined edges can be obtained as seen from Figure 8(b) since the excess liquid is effectively removed during printing, demonstrating the effectiveness of the liquid-absorbing system in improving the printing resolution.

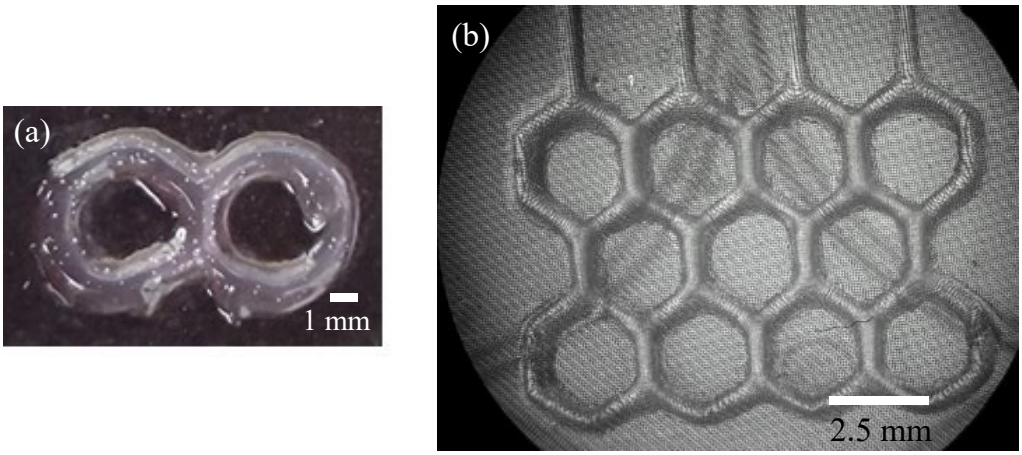

Figure 8. Comparison of printed (a) annular shape [22] (Reprinted (adapted) with permission from ACS Biomater. Sci. Eng. Copyright 2017 American Chemical Society) and (b) honeycomb structures

3.2.2. Tubular structure

Printing tubular structures with a high aspect (height-diameter) ratio is of great interest due to the necessity of such tubular structures for various biomedical needs such as vasculature-like applications. The liquid-absorbing system helps successfully remove the excess liquid along the entire printing process. During the printing of the first few layers that become the base of a structure, it is important that the material is deposited not only at a controlled manner without excess liquid interfering with the deposition location, but also ensuring a homogeneous and smooth surface for future layers to be built upon. Additionally, during the printing of successive layers excess liquid flows towards the structure base and is drained away by the liquid-absorbing system. As such, tubular structures with a 3 or 5 mm diameter were printed with a higher height-diameter ratio than that previously obtained without the liquid-absorbing system. As seen from Figure 9, the achievable height-diameter ratio during intersecting jets printing of alginate in air can be increased from 0.5 to 2.5, a five-time increase when compared to a previous study [22]. It demonstrates the promising fabrication capability of intersecting jets printing in air, which can be utilized for direct biofabrication in air for patients in need.

	Without the liquid-absorbing system	With the liquid-absorbing system
Aspect ratio (Height vs. diameter)	≈ 0.5	≈ 2.5
Top view	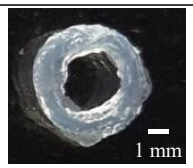	
Side view		

Figure 9. Comparison of printed tubular structures without [22] (Reprinted (adapted) with permission from ACS Biomater. Sci. Eng. Copyright 2017 American Chemical Society) and with the liquid-absorbing system

3.2.3. Conical structure

Furthermore, 5.0 mm diameter hollow conical structures were designed and printed to prove that small overhang and hollow features can be also printed using the proposed technology. In this study, slope angles smaller than 30° were adopted to avoid potential structure collapse. Figure 10(a) shows the computer-aided design (CAD) model of the design, whereas Figure 10(a1) and (a2) shows different views of a printed structure. In order to confirm the structural integrity of the printed structure, blue dye was filled into the hollow cavity of the conical structure and no dye leaking is observed as seen from Figure 10(a3). These results show how structures with lumens and hollows can be printed on liquid-absorbing substrates. Higher aspect ratio conical

structures (such as 2:1) can also be printed as seen from Figure 10(e), demonstrating the self-supporting printing potential of the proposed technology.

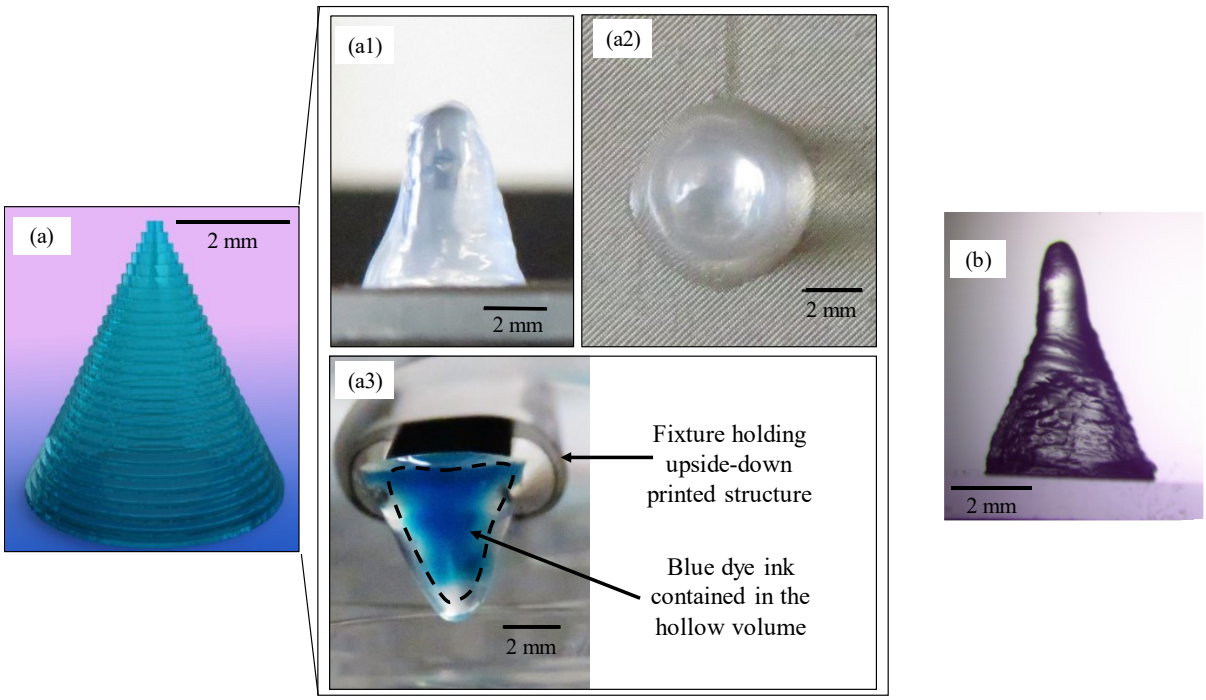

Figure 10. Printed conical structure (a) design, (a1) side view, (a2) top view, (a3) upside down structure containing blue dye ink to demonstrate its structural integrity, and (b) a higher aspect ratio construct

3.3. Effect on cell viability and morphology

For bioprinting of living cells, the post-printing cell viability is of great concern for the adoption of a printing technology. Figure 7(c) and (d) shows some printed 3T3 cellular tubes with a 5.0 mm diameter and a 1.5 mm height without and with the liquid-absorbing system. To have the same tube height, an additional 70 layers were printed when using the absorption system.

The printing process took approximately 10 minutes when not using the liquid-absorbing system and 30 minutes when using the liquid-absorbing system, respectively, and then the printed cellular constructs were cultured accordingly. As seen from Figure 11(a), the 3T3 cells can survive the printing process without and with the liquid-absorbing system, and the resulting cell viability is around 80% or higher during the culturing duration. For a better comparison, Fig. 11 (b1) and (b2) present live-dead staining of the post-printing 3T3 cells, with and without the liquid-absorbing system was used, respectively, after 3 days of culturing. Most of the stained cells show green fluorescence in both cases, indicating living cells, while only a few cells show red fluorescence as an indication of being dead. There is no statistical difference when the liquid-absorbing system is or is not used, meaning that even with printing using the liquid-absorbing system removing excess water during the process, there is enough supply of oxygen and nutrients to the printed cells. The excess liquid flows down toward the liquid-absorbing layer due to wetting and gravity, and this liquid flow might also contribute to the re-distribution of water with oxygen and nutrients to the already built layers, preventing dryness from happening.

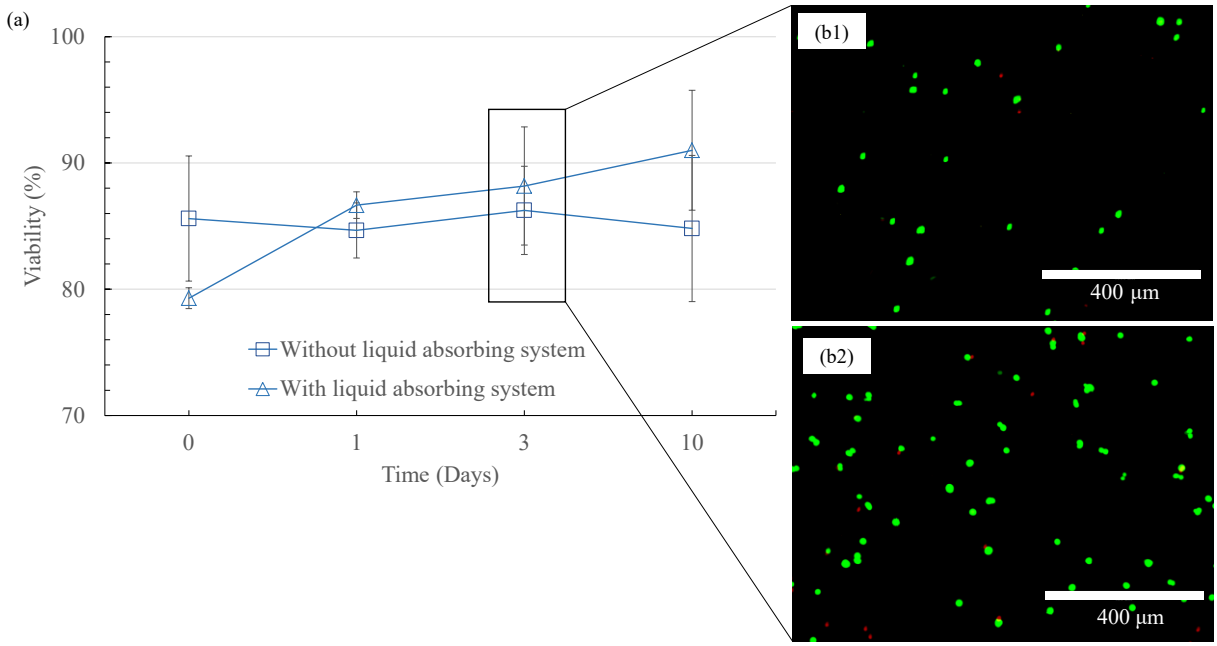

Figure 11. (a) Cell viability results (Insets: fluorescent cell images for (b1) with and (b2) without liquid-absorbing system)

The morphology of post-printing cells can be seen in Figure 12. More spindle-shaped living cells in a greater concentration are observed with the presence of a liquid-absorbing system (Fig. 12 (a)) after ten days of culturing. This might be attributed to the enhanced cell-cell interaction when the liquid-absorbing system is used, which wicks away excessive water during printing and results in a condensed construct. The proximity of cells might increase the interaction of communication materials such as cytokines and chemokines within the cells, promoting their positive morphological changes.

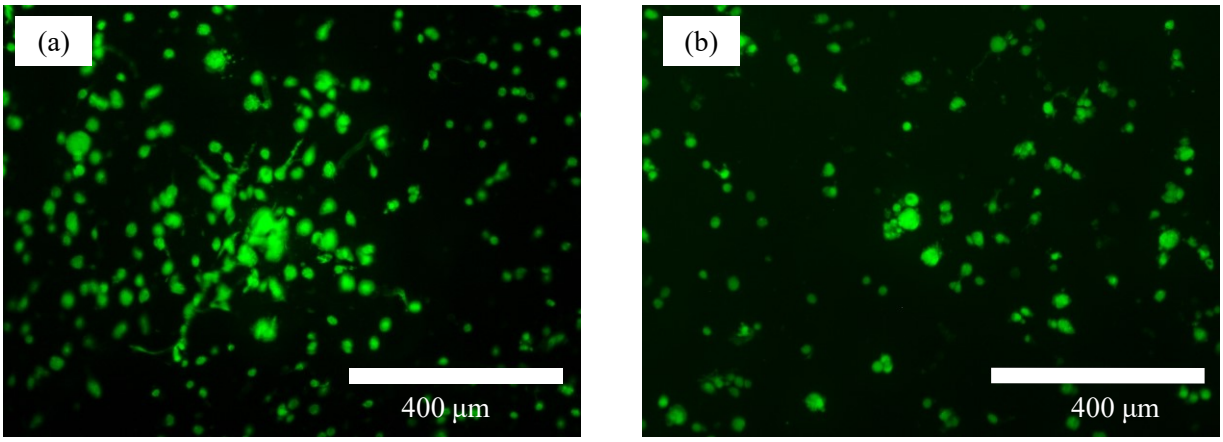

Figure 12. Living cells (shown in green) printed (a) with and (b) without a liquid-absorbing system after ten-day post-printing culturing

3.4 Discussion

The presented technology can facilitate the printing of reactive materials, which are not printable using other conventional additive manufacturing technologies because of the unfavorable rheological properties of reactive materials after mixing. Since the objective of this study is to improve the performance of intersecting jets–based reactive material printing, the general printing performance and capabilities are not compared with those of other processes including extrusion-based processes such as co-extrusion. While co-extrusion may be used to print reactive materials, the mixing performance is limited due to its passive mixing nature even though a stirrer is included as part of an extruder. For the presented intersecting jets technologies, the mixing is voxel-by-voxel based, guaranteeing a satisfactory mixing performance as reported [30]. Compared with extrusion, material jetting-based technologies such as intersecting jets printing have some advantages in terms of large direct writing height (meaning a large workspace) and high printing resolution (voxel-by-voxel vs. filament-by-filament).

Sodium alginate is a common material for bioinks due to its wide applicability as a versatile biomaterial, so sodium alginate and calcium chloride are selected as examples of reactive materials for feasibility demonstration of the presented technology. Apart from these examples, the presented technology can be applied to print any other reactive materials, which may not be readily printable by other additive manufacturing technologies. More complicated constructs will be printed using additional support structures as needed in a future study.

4. Conclusions and future work

This study demonstrates the improved fabrication capability that a liquid-absorbing system brings to intersecting jets printing. The liquid-absorbing system is comprised of a stainless-steel wire mesh and fibrous tissue paper. By selecting a wire mesh with a proper size, 80 and 100, the proposed liquid-absorbing system can absorb up to 65-90% of the excess liquid (water) resulting from printing aqueous reactive sodium alginate and calcium chloride inks. The absorption speed decreases with printing time since the tissue paper is not replaced in the proposed system and may start saturating over time. By controlling the tilt angles of intersecting jets, the incident angle of post-collision droplets is desirable to be less than 14º to avoid droplet bouncing on the top of the previously deposited layer during 3D bioprinting. Using the liquid-absorbing system, different 3D structures have been successfully printed using intersecting jets printing since excess fluid is effectively removed during the printing process. For tubular alginate constructs printed in air from sodium alginate and calcium chloride inks, a 2.5 height-diameter ratio can be achieved. The proposed printing technology does not influence the post-printing cell viability during printing 3T3 cells, demonstrating its promising potential for bioprinting applications.

Future work may include as follows: 1) the analytical investigation of the effects of ink composition and rheological properties on the printing performance when using the liquid-absorbing system during intersecting jets printing, 2) modeling and optimization of the performance of the liquid-absorbing system, 3) additional process innovation in order to fabricate higher complexity structures, and 4) tissue engineering applications of the proposed bioprinting technology. It is noted that direct printing of cellular constructs in air has promising clinical applications, which may be enabled using the proposed liquid-absorbing system for processes based on intersecting jets printing technologies.

Acknowledgements

This study was partially supported by the US National Science Foundation (CMMI-1634755), and the cell culture work was supported by Wenxuan Chai of the University of Florida.

Statement on conflicts of interest

One of the authors of this article is part of the Editorial Board of the journal. To avoid potential conflicts of interest, the responsibility for the editorial and peer-review process of this article lies with the journal's other editors. Furthermore, the authors of this article were removed from the peer review process and had no, and will not have any access to confidential information related to the editorial process of this article.

Competing financial interests

D.B.W is an employee of MicroFab Technologies.

References

[1] J.P. Kruth, M.C. Leu, T. Nakagawa, Progress in Additive Manufacturing and Rapid Prototyping, CIRP Annals- Manufacturing Technology Vol. 47(2) (1998) 525–540. https://doi.org/10.1016/S0007-8506(07)63240-5.

[2] I. Gibson, D.W. Rosen, and B. Stucker, Additive Manufacturing Technologies: Rapid Prototyping to Direct Digital Manufacturing, Springer, New York, NY, 2010.

[3] Y. Huang, M.C. Leu, J. Mazumder, A. Donmez, Additive Manufacturing: Current State, Future Potential, Gaps and Needs, and Recommendations, ASME J. of Manufacturing Sci. and Eng. Vol. 137(1) (2015) 014001. https://doi.org/10.1115/1.4028725.

[4] D. Rejeski, F. Zhao, Y. Huang, Research Needs and Recommendations on Environmental Implications of Additive Manufacturing, Additive Manufacturing Vol. 19 (2018) 21-28. https://doi.org/10.1016/j.addma.2017.10.019.

[5] Y. Huang, S. R. Schmid, Additive Manufacturing for Health: State of the Art, Gaps and Needs, and Recommendations, ASME Journal of Manufacturing Science and Engineering Vol. 140(9) (2018) 094001-1-11. https://doi.org/10.1115/1.4040430.

[6] V. Tsang, A. Chen, L. Cho et al., Fabrication of 3D hepatic tissues by additive photopatterning of cellular hydrogels. The FASEB Journal Vol. 21(3) (2007) 790-801. https://doi.org/10.1096/fj.06-7117com.

[7] J. Nichol, A. Khademhosseini, Modular Tissue engineering: engineering biological tissues from the bottom up, Soft Matter Vol. 5(7) (2009) 1312. https://doi.org/10.1039/b814285h.

[8] N. Fedorovich, J. De Wijn, A. Verbout, J. Alblas, W. Dhert, Three-Dimensional Fiber Deposition of Cell-Laden, Viable, Patterned Constructs for Bone Tissue Printing, Tissue Engineering Vol. 14(1) (2008) 127-133. https://doi.org/10.1089/ten.a.2007.0158.

[9] Y. Jin, C. Liu, W. Chai, A. Compaan, Y. Huang, Self-Supporting Nanoclay as Internal Scaffold Material for Direct Printing of Soft Hydrogel Composite Structures in Air, ACS Applied Materials & Interfaces Vol. 9(20) (2017) 17456-17465. https://doi.org/10.1021/acsami.7b03613.

[10] Y. Jin, A. Compaan, W. Chai, Y. Huang, Functional Nanoclay Suspension for Printing-then-Solidification of Liquid Materials, ACS Applied Materials & Interfaces Vol. 9(23) (2017) 20057-20066. https://doi.org/10.1021/acsami.7b02398.

[11] B. Guillotin, A. Souquet, S. Catros et al., Laser assisted bioprinting of engineered tissue with high cell density and microscale organization, Biomaterials Vol. 31(28) (2010) 7250-7256. https://doi.org/10.1016/j.biomaterials.2010.05.055.

[12] R. Xiong, Z. Zhang, W. Chai, Y. Huang, D. Chrisey, Freeform drop-on-demand laser printing of 3D alginate and cellular constructs, Biofabrication Vol. 7(4) (2015) 045011. https://doi.org/10.1088/1758-5090/7/4/045011.

[13] W. Wilson, T. Boland, Cell and organ printing 1: Protein and cell printers, Anat. Rec. Vol. 272A(2) (2003) 491-496. https://doi.org/10.1002/ar.a.10057.

[14] M. Nakamura, A. Kobayashi, F. Takagi et al., Biocompatible Inkjet Printing Technique for Designed Seeding of Individual Living Cells, Tissue Eng. Vol. 11(11-12) (2005) 1658-1666. https://doi.org/10.1089/ten.2005.11.1658.

[15] T. Boland, X. Tao, B. Damon, C. Xiaofeng, Application of inkjet printing to tissue engineering, Biotechnology Journal: Healthcare Nutrition Technology Vol. 1(9) (2006) 910-917. https://doi.org/10.1002/biot.200600081.

[16] C. Xu, W. Chai W, Y. Huang, R. Markwald, Scaffold-free inkjet printing of three-dimensional zigzag cellular tubes, Biotechnol. Bioeng. Vol. 109(12) (2012) 3152-3160. https://doi.org/10.1002/bit.24591.

[17] K. Christensen, C. Xu, W. Chai, Z. Zhang, J. Fu, Y. Huang, Freeform inkjet printing of cellular structures with bifurcations, Biotechno.l Bioeng. Vol. 112(5) (2015) 1047-1055. https://doi.org/10.1002/bit.25501.

[18] C. Visser, T. Kamperman, L. Karbaat, D. Lohse, M. Karperien, In-air microfluidics enables rapid fabrication of emulsions, suspensions, and 3D modular (bio)materials, Sci. Adv. Vol. 4(1) (2018) eaao1175. https://doi.org/10.1063/1.1888026.

[19] N. Reis, C. Ainsley, B. Derby. Ink-jet delivery of particle suspensions by piezoelectric droplet ejectors, J. Appl. Phys. Vol. 97(9) (2005) 094903. https://doi.org/10.1063/1.1888026.

[20] T. Xu, J. Jin, C. Gregory, J. Hickman, T. Boland, Inkjet printing of viable mammalian cells, Biomaterials Vol. 26(1) (2005) 93-99. https://doi.org/10.1016/j.biomaterials.2004.04.011.

[21] B. Derby, Bioprinting: inkjet printing proteins and hybrid cell-containing materials and structures, J Mater Chem.Vol. 18(47) (2008) 5717. https://doi.org/10.1039/b807560c.

[22] K. Christensen, A. Compaan, W. Chai, G. Xia, Y. Huang, In Situ Printing-then-Mixing for Biological Structure Fabrication Using Intersecting Jets, ACS Biomater. Sci. Eng. Vol. 3(12) (2017) 3687-3694. https://doi.org/10.1021/acsbiomaterials.7b00752.

[23] Y. Yeo, A. U. Chen, O. A. Basaran,; K. Park, Solvent exchange method a novel microencapsulation technique using dual microdispensers, Pharm. Res. Vol. 21 (8) (2004) 1419−1427. https://doi.org/10.1023/B:PHAM.0000036916.96307.d8.

[24] A. Skardal, D. Mack, E. Kapetanovic et al., Bioprinted amniotic fluid‐derived stem cells accelerate healing of large skin wounds, Stem cells translational medicine Vol. 1(11) (2012) 792-802. https://doi.org/10.5966/sctm.2012-0088.

[25] V. Lee, G. Singh, J. Trasatti et al., Design and Fabrication of Human Skin by Three-Dimensional Bioprinting, Tissue Engineering Part C: Methods. Vol. 20(6) (2014) 473-484. . https://doi.org/10.1089/ten.tec.2013.0335.

[26] S. Khalil, W. Sun, Bioprinting Endothelial Cells With Alginate for 3D Tissue Constructs, J. Biomech. Eng. Vol. 131(11) (2009) 111002. https://doi.org/10.1115/1.3128729.

[27] S. V. Murphy, A. Skardal, A. Atala, Evaluation of hydrogels for bio-printing applications, J. Biomed. Res. Part A Vol. 101A (1) (2013) 272-274. https://doi.org/10.1002/jbm.a.34326.

[28] T. Boland, T. Xu, B.J. Damon, B. Manley et al., Drop on demand printing of cells and materials for designer tissue constructs Mater, Sci. Eng. C Vol. 27(3) (2007) 372-376. https://doi.org/10.1016/j.msec.2006.05.047.

[29] K. Christensen, Y. Huang, Study of Layer Formation during Droplet-Based 3D Printing of Gel Structures, ASME J. of Manufacturing Sci. and Eng. Vol. 139(9) (2017) 091009-1-8. https://doi.org/10.1115/1.4036785.

[30] K. Christensen, Layer Formation and Deformation Compensation during Inkjet Printing of 3D Biological Structures, Ph.D. Dissertation, University of Florida, Gainesville, FL (2017).

[31] Y. Couder, E. Fort, C. Gautier, A. Boudaoud, From Bouncing to Floating: Noncoalescence of Drops on a Fluid Bath, Phys. Rev. Lett. Vol. 94(17) (2005) 177801. https://doi.org/10.1103/physrevlett.94.177801.

[32] J. Zou, P. Wang, T. Zhang, X. Fu, X. Ruan, Experimental study of a drop bouncing on a liquid surface, Physics of Fluids Vol. 23(4) (2011) 044101. https://doi.org/10.1063/1.3575298.

[33] C. Gouiller, A. Guittonneau, L. Jacquot, Generation and trajectory control of water drops able to bounce on a flat water surface, Emergent Scientist Vol. 1 (2017) 1. https://doi.org/10.1051/emsci/2017001.

[34] K. Pan, Y. Tseng, J. Chen, K. Huang et al., Controlling droplet bouncing and coalescence with surfactant, J. Fluid Mech. Vol. 799 (2016) 603-636. https://doi.org/10.1017/jfm.2016.381.